Available online at www.sciencedirect.com
SCIENCE DIRECT®

Journal of the European Ceramic Society 24 (2004) 2131–2139
www.elsevier.com/locate/jeurceramsoc

# Unreinforced and carbon fibre reinforced hydroxyapatite: resistance against microabrasion

Annett Dorner-Reisel[a,*], Karl Berroth[b], Rainer Neubauer[b], Klaus Nestler[c], Günter Marx[c], Magdalena Scislo[d], Eberhard Müller[a], Anna Slosarcyk[d]

[a]*Institute of Ceramic Materials, Technische Universität Bergakademie Freiberg, Gustave-Zeuner Stasse 3, Freiberg 09596, Germany*
[b]*FCT Ingenieurkeramik GmbH, Rauenstein, Germany*
[c]*Technical University of Chemnitz, Germany*
[d]*University of Mining and Technology Cracow, Poland*

Received 15 February 2003; accepted 10 May 2003

**Abstract**

Hot pressing (1000–1150 °C, 25 MPa, 15 min, argon atmosphere) was used to process unreinforced and carbon short fibre reinforced hydroxyapatite (20% fibre volume fraction). Due to the selected processing parameters, a fine grained crystalline calcium hydroxyapatite matrix without any decomposition products and a close contact between the slightly curved surface of the carbon fibres and the hydroxyapatite was realized. The nano- and microstructure of the hydroxyapatite and the composites is characterized by Fourier transformed infrared spectroscopy, Raman spectroscopy, X-ray diffraction and high resolution transmission electron microscopy. Ball-crater wear tests were performed with abrasive SiC particles to assess the sensitivity against microabrasion. The reinforcement of calcium hydroxyapatite with carbon short fibres enhances the resistance against microabrasion. An additional 60 nm thick pyrolytic carbon coating on the fibres further improves the wear resistance due to prevention of the crack formation, which can be induced by thermal expansion mismatch between reinforcement and matrix.


*Keywords:* Bioceramics; Carbon fibres; Composites; Hydroxyapatite; Interfaces; Microstructure; Wear resistance

## 1. Introduction

Calcium hydroxyapatite bioceramic is applied as a coating on metallic prostheses in order to improve their biocompatibility. Recent results from orthopaedic implantation of hydroxyapatite coated hips lead to the conclusion that the hydroxyapatite bony bonding secures the implant.[1] The majority of hydroxyapatite coatings are deposited by the plasma spraying technique. Fu et al.[2] gave evidence of the essential influence of the microstructure of such hydroxyapatite coatings on their wear resistance. They suggest a post-treatment of plasma sprayed coatings like hot isostatic pressing (HIP) to densify the microstructure, decrease the generation of wear debris and mitigate the wear. Changing the microstructure of hydroxyapatite bioceramic is also an important measure to expand the applicability of the ceramic further. Due to the brittleness of synthetic calcium hydroxyapatite, the bioceramic is only applicable as a coating or under nonload bearing conditions. However, because of the excellent biocompatibility of hydroxyapatite, there are extensive efforts to improve also its own mechanical properties. One possible method is reinforcement with particles,[3–5] short or long fibres.[6–8] Reinforced hydroxyapatite is expected to have a considerably changed wear resistance in comparison to the unreinforced bioceramic. Although, the wear resistance of artificial materials in the body is of high relevance, the tribological properties of hydroxyapatite-based composites are only lightly illuminated at present. The following study correlates the microstructure of carbon fibre reinforced hydroxyapatite to the resistance of the bioceramic against microabrasion. In addition to modified processing parameters, the fibre–matrix interface is tailored by a pyrolytic carbon coating.

* Corresponding author. Tel.: +49-3731-39-2085; fax: +49-3731-39-3662.
*E-mail address:* dorner@ikw.tu-freiberg.de (A. Dorner-Reisel).

0955-2219/03/$ - see front matter © 2003 Elsevier Ltd. All rights reserved.
doi:10.1016/S0955-2219(03)00373-X

## 2. Experimental procedure

### 2.1. Processing of unreinforced and carbon fibre reinforced hydroxyapatite ceramics

The starting materials for the processing of unreinforced and fibre reinforced hydroxyapatite are commercial hydroxyapatite powder (2196, company Merck, Germany) and carbon fibres of the type T 800 H (company Toray, Japan). The fibres are supplied as endless bundles. An initial step of fibre desizing, a thermal treatment under protective atmosphere in order to remove the epoxy sizing on the fibres, is carried out. A pyrolytic carbon coating (pyC) of 60 nm thickness is deposited on a set of the endless fibres by chemical vapour deposition (CVD) using gaseous hydrocarbon, e.g. touloene, as a precursor.[9] Subsequently, the endless uncoated and pyC-coated carbon fibres are cut into short fibres with a length of between 20 and 150 μm. The fibre cutting is carried out in a planetary ball mill (Fritsch ball mill) with 5 g fibres and 10 $SiO_2$ balls with a diameter of 20 mm. The ball surfaces were roughened before the cutting process by milling them for 10 min with abrasive SiC particles. The roughened balls and the fibres were placed in 250 ml $SiO_2$ cups and exposed to a high rotation speed (step 8.5). The reached length of the short fibres depends on the duration of the milling time. For a fibre length of between 20 and 150 μm, a milling time of 90 s is necessary.

Both, the hydroxyapatite powder and the uncoated or the pyC-coated short fibres are mixed in a planetary ball mill under gentle conditions. In the 250 ml cups, 17 g hydroxyapatite and 2.28 g fibres (20 vol.% fibre reinforcement) as well as five $SiO_2$ balls without a roughened surface are given. A homogeneous powder mixture (Fig. 1) is reached after 3 min mixing at rotation step 3.

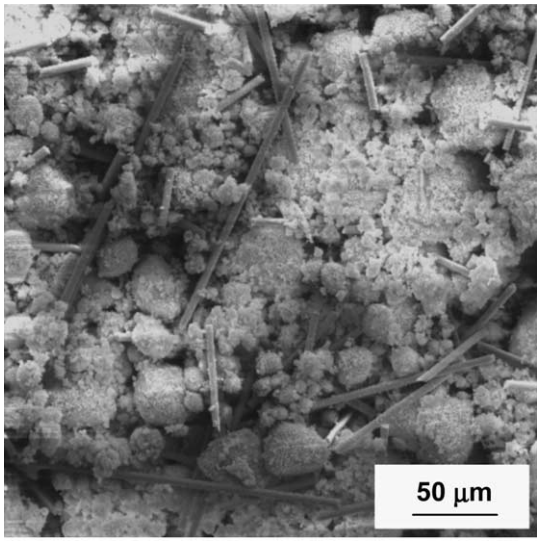


Fig. 1. Powder mixture of 20 vol.% carbon fibres and hydroxyapatite, SEM.

Finally, bioceramic samples of cylindrical shape of 10 mm high and 30 mm diameter were sintered by hot pressing under argon atmosphere in a hydraulic press. The powder mixtures were added as loose powders to the dies and heated up with a heating rate of 15 °C/min to the sintering temperature of 1000, 1075 or 1150 °C. After the sintering temperature was reached, the loading with 25 MPa pressure took place for a time of 15 min. Cooling rate of the samples was 30 °C/min. Using the described parameters, ceramic cylinders of unreinforced hydroxyapatite, hydroxyapatite with uncoated fibres and hydroxyapatite with pyC-coated fibres were processed.

### 2.2. Characterisation of the microstructure

Phase identification of the unreinforced and carbon fibre reinforced hydroxyapatite was performed using the X-ray diffractometer URD 63 (company Seifert-FPM). A diffraction angle range $2\theta$ of between 10 and 80 ° was used with a step width of 0.05 ° and a measurement time of 15 s by applying Co-radiation. Fourier transformed infrared spectroscopy was performed with a spectrometer of the type Nicolet 510 at room temperature. The spectra were recorded after the sintering process on pulverized samples. The bioceramics were ground. The bioceramic powder (1.5 mg) was mixed with 450 mg KBr and pressed to pellets in an evacuated die with a pressure of 25 MPa. Of this mixture 250 mg served as material for recording FT-IR spectra. Furthermore, Raman spectroscopy was carried out at room temperature with a spectrometer of the type Jobin Yvon T 64000. In the quasi-back scattering geometry of an $Ar^+$ laser operating with a power of 200 mW, the hot pressed samples were proven with 5 mW of the 514,5 nm line over a spot of about 2 μm. The scanning electron microscopy (SEM) investigations were made with a Carl Zeiss DSM 960 apparatus. SEM investigations were carried out at a voltage of 15 kV. For high resolution transmission electron microscopy (HR-TEM), a Jeol JEM 2010 FEF with an accelerating voltage of 200 kV was used. Before the nano-structure of the materials was characterised, thin samples were prepared by mechanical and ion thinning. For better interpretation of the mechanical properties, the porosity of the samples were determined by quantitative analysis on polished surfaces using light microscopy. On each sample, 10 measurement fields of (250×250) $\mu m^2$ were evaluated.

### 2.3. Microabrasion by ball-crater wear and hardness

The hardness of the samples was assessed with a Vickers type diamond indenter using a Fischerscope H100. The final load amounted to 1 N. Each sample was tested 10 times for calculating the mean value and the standard deviation. Before mechanical testing, the

surface of the samples was polished up to a finish of 1 μm with diamond paste.

Wear experiments were performed with a ball-crater apparatus, the Calowear tester (CSEM Instruments, Switzerland). Hereby, the abrasive wear of the samples is caused by an abrasive fluid which consists of distilled water and SiC-particles with an average diameter of about 4 μm. This fluid is constantly supplied and dripped on the balls surface. Due to the rotation of the steel ball (diameter: 30 mm, sliding speed: 0.22 m $s^{-1}$), the abrasive fluid forms a continuous film on it. The weight and the rotation of the ball transfers a normal and a tangential force on the SiC particles which are able to penetrate into the worn surface, scratching it and removing material. For every measurement the sliding distance was 33.3±0.07 m and the acting normal force approximately 400 mN; which can be determined by a loading cell beneath the sample (see Fig. 2). The geometry of the formatted spherical wear crater is measured and used for the calculation of the wear coefficient $k$. On every sample three measurements were carried out. The wear coefficient $k$ can be calculated according Eq. (1).

$$k = \frac{\pi b^4}{32 L d F_N} \quad (1)$$

$k$—wear coefficient ($mm^2$ $N^{-1}$), $d$—diameter of the rotating ball (mm), $b$—diameter of the spherical wear crater (mm), $L$—wear way (mm), $F_N$—normal force (N).

## 3. Results

### 3.1. Micostructural characterisation

Figs. 3 and 4 show SEM images of hydroxyapatite with uncoated and hydroxyapatite with pyC-coated carbon fibres. Although, there is no fibre agglomeration, the distribution of the reinforcement is not completely homogeneous. The polished cross-sections also reveal the remaining porosity. Furthermore, in composites with uncoated carbon fibres, a crack net is evident which was not observed in the composites with pyC-coated carbon fibres.

From X-ray diffraction, no decomposition of the hydroxyapatite matrix or reaction product between the carbon fibres and the calcium phosphate matrix were detected after hot pressing the unreinforced and the fibre reinforced hydroxyapatite at temperatures of between 1000 and 1150 °C for 15 min (Fig. 5). The XRD spectra matches with the ICDD PDF No. 9-432

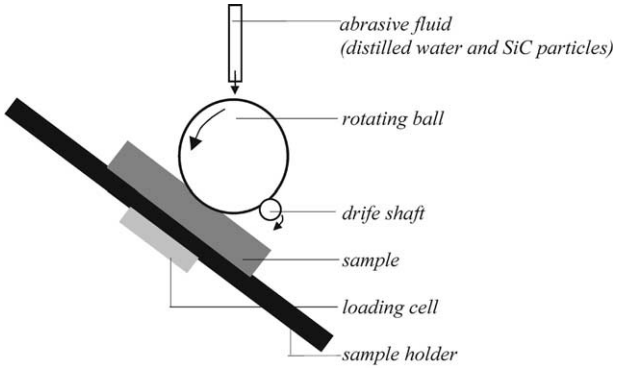


Fig. 2. Schematic of the apparatus used for measuring the micro-abrasion (CSEM Instruments, Switzerland).

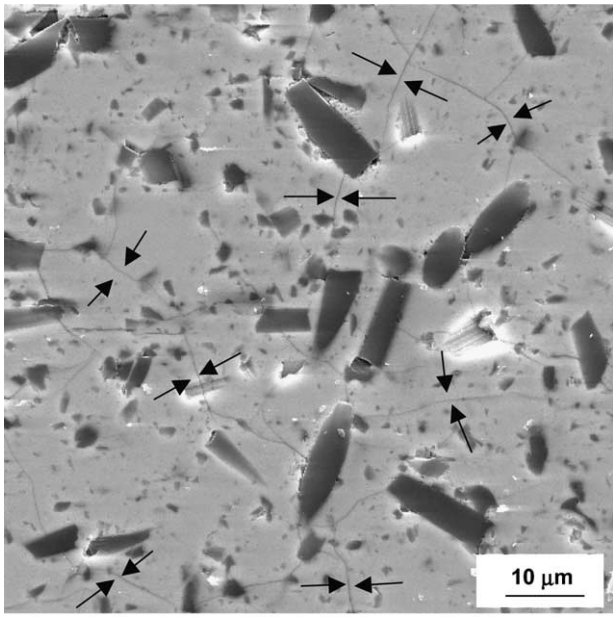


Fig. 3. Polished surface of hydroxyapatite reinforced with uncoated carbon fibres after hot pressing at 1000 °C: crack net → ←, SEM.

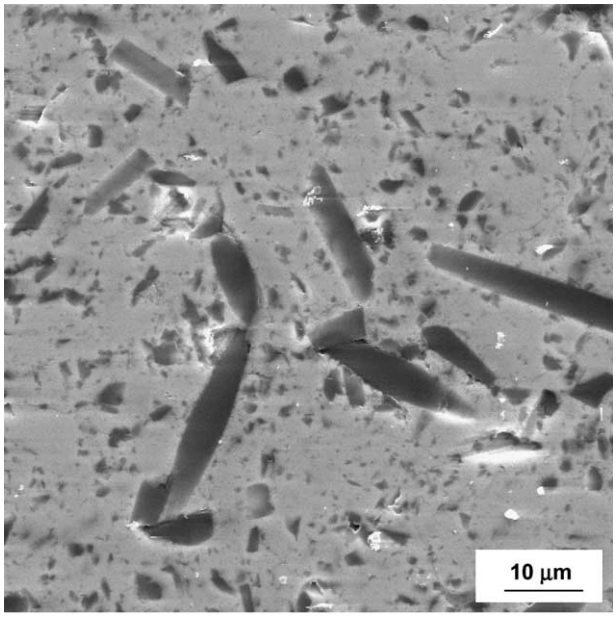


Fig. 4. Polished surface of hydroxyapatite reinforced with pyC-coated carbon fibres after hot pressing at 1000 °C, SEM.

for calcium hydroxyapatite exactly. No additional phases were detected. Infrared spectroscopy confirms a similar composition of both, unreinforced and fibre reinforced hydroxyapatite (Figs. 6 and 7). In addition to $PO_4^{3-}$, O–P–O and $OH^-$ as well as H–O–H, the IR-spectra of all samples give evidence of the presence of $CO_3^{2-}$ (absorption bands at 1420 and 878 $cm^{-1}$) which can substitute OH-groups in the calcium hydroxyapatite lattice. The high crystallinity of all samples is proven by the splitting of the band between 1040 and 1100 $cm^{-1}$. For unreinforced hydroxyapatite, the IR-spectra do not change with hot pressing temperature (Fig. 6). However, for both the hydroxyapatite reinforced with uncoated carbon fibres and that with pyC-coated carbon fibres, the intensity of the lines around 3500 and 1600 $cm^{-1}$ decreases with increasing sintering temperature. This confirms the evaporation of crystal water from the calcium phosphate matrix of the composites

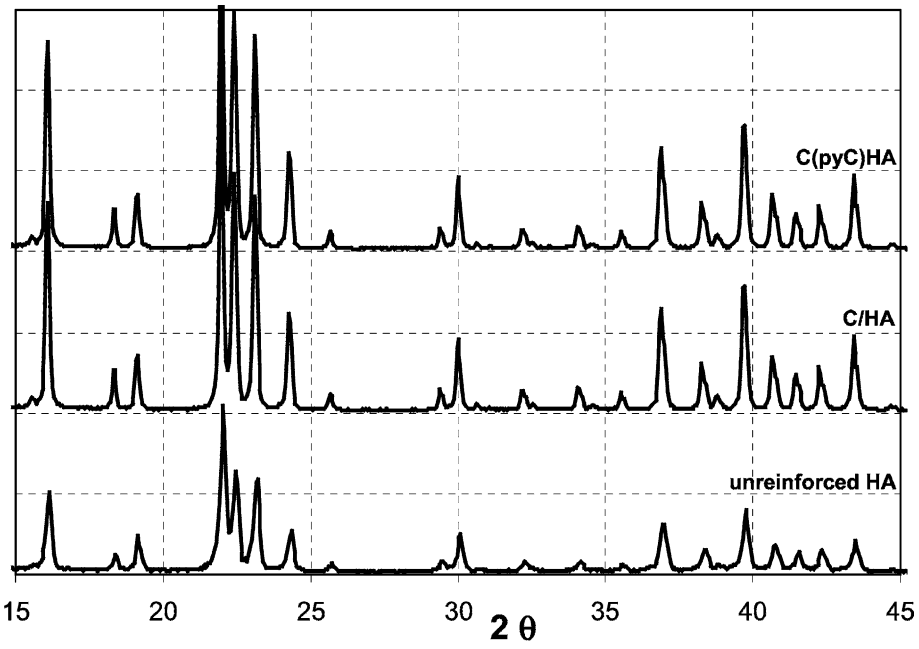


Fig. 5. X-ray diffraction patterns of unreinforced hydroxyapatite, hydroxyapatite with 20 vol.% carbon fibres and hydroxyapatite with 20 vol.% pyC-coated carbon fibres after hot pressing at 1150 °C.

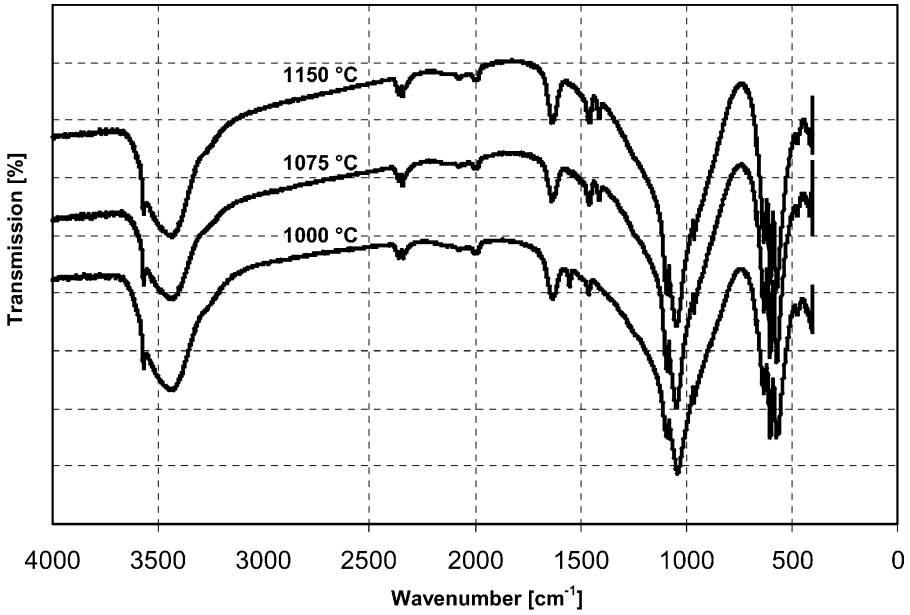


Fig. 6. FT-IR spectra of unreinforced hydroxyapatite sintered at 1000, 1075 and 1150 °C.

with increasing hot pressing temperature to an extent that is not reached by the unreinforced hydroxyapatite. The Raman spectra of all samples exhibit peaks at 964 $cm^{-1}$ (symmetrical phosphate stretching) and 3575 $cm^{-1}$ (OH stretching). The 964 $cm^{-1}$ peak is sharp and of high intensity which points to high crystallinity and phase purity. In addition to hydroxyapatite, no other calcium phosphates were detected by Raman spectroscopy. In the samples with carbon fibre reinforcement (Fig. 8), the $sp^2$-hybridized carbon gives additional peaks at 1357 and 1596 $cm^{-1}$. For both, the C/HA- and the C(pyC)/HA-composites a very fine grained matrix,

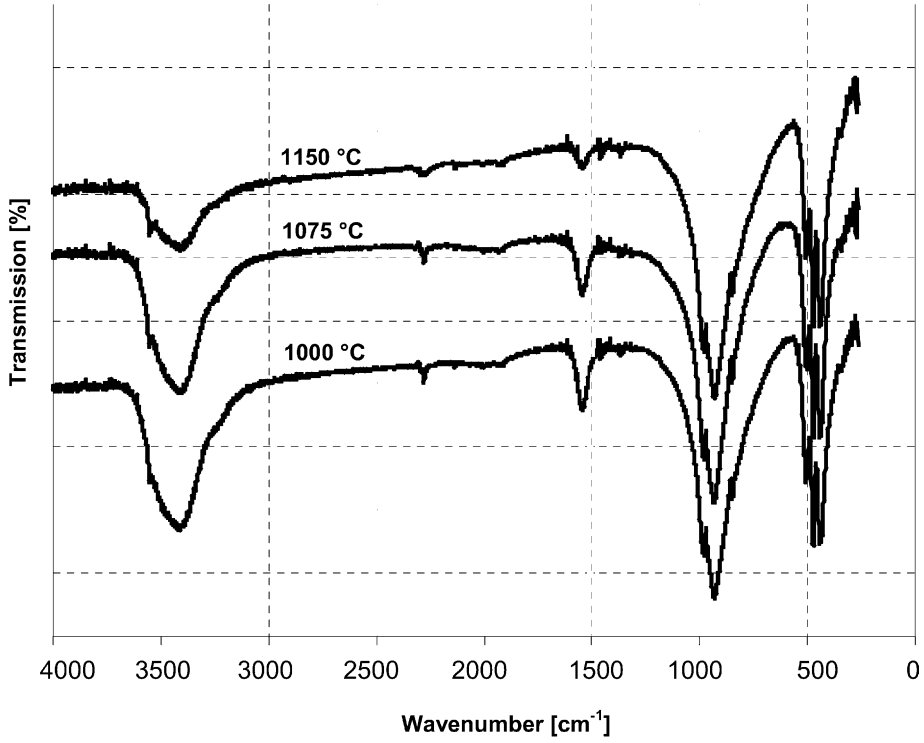


Fig. 7. FT-IR spectra of unreinforced hydroxyapatite sintered at 1000, 1075 and 1150 °C.

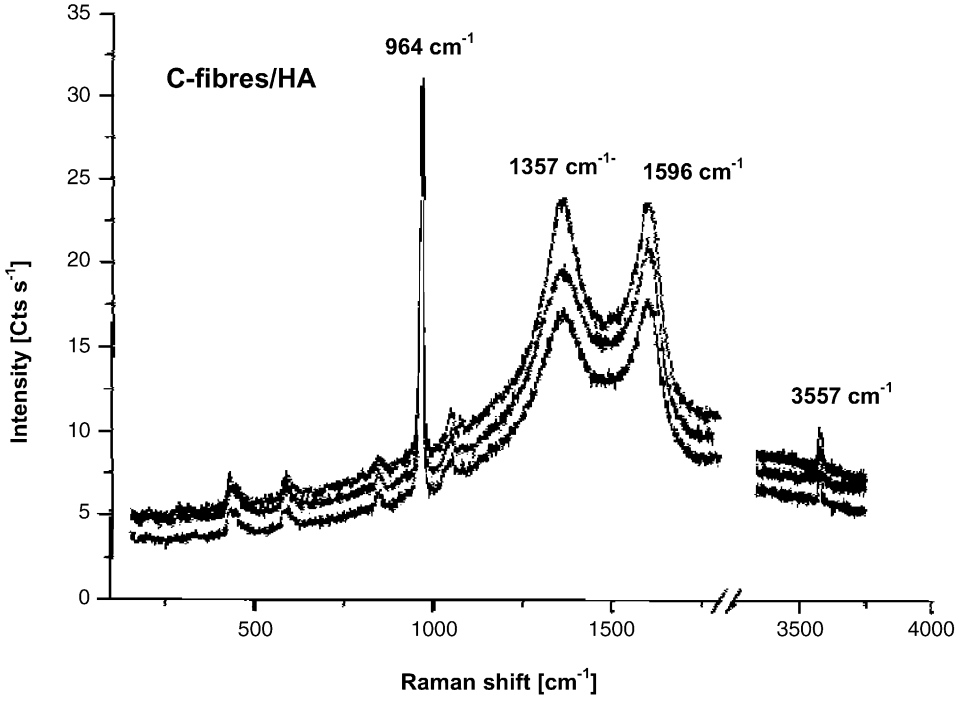


Fig. 8. Raman spectra of the carbon fibre reinforced hydroxyapatite sintered at 1000, 1075 and 1150 °C.

excellent fibre–matrix contact without microspaces at the interface and no reaction products were observed by TEM (Figs. 9 and 10). In C/HA and C(pyC)/HA composites, "void type" defects within the hydroxyapatite grains are located some 10 nm away from the fibre–matrix interface (Fig. 11).

### 3.2. Wear behaviour under microabrasive conditions

Two essential influences on the hardness of hydroxyapatite are porosity and grain size. As the grains are in the nano-meter scale for all tested materials, a positive effect on the hardness is expected. For the unreinforced hydroxyapatite the porosity was of 3.5±0.18% after hot pressing at 1000 °C, 3.1±0.19% after sintering at 1075 °C and 0.5±0.09% after hot pressing at 1150 °C. For hydroxyapatite, a sintering temperature for reaching maximum density has been proposed.[10] Above this temperature, the calcium hydroxyapatite starts to decompose which results in a rapidly decreasing density. As confirmed by the microstructural investigations, decomposition of the hydroxyapatite did not occur under the chosen process parameters. In accordance to the unreinforced hydroxyapatite, the measured porosity of carbon fibre reinforced materials declines from 2.9±0.92% after hot pressing at 1000 °C to 0.7±1.4% after hot pressing at 1150 °C with only minor differences to the composites with pyC-coated fibres.

The hardness of the hydroxyapatite with 20 vol.% carbon fibres is of between 0.34 and 0.53 GPa and about one half lower in comparison with the hardness of the unreinforced ceramic which is between 0.74 and 0.63 GPa (Table 1). The distance is attributed to the much lower resistance of $sp^2$-hybridised carbon against the indentation of the Vickers diamond.

Although, the hardness of the reinforced hydroxyapatites is lower in comparison with the unreinforced calcium phosphate ceramic, the resistance against microabrasion of the composites is improved. As evident from Table 1 and Fig. 12, the wear resistance of the hydroxyapatite with uncoated carbon fibres increases by about 50% in comparison to the unreinforced ceramic, while composites with pyC-coated fibres show even better results. The wear coefficient of this composites is reduced up to 90% in comparison with unreinforced

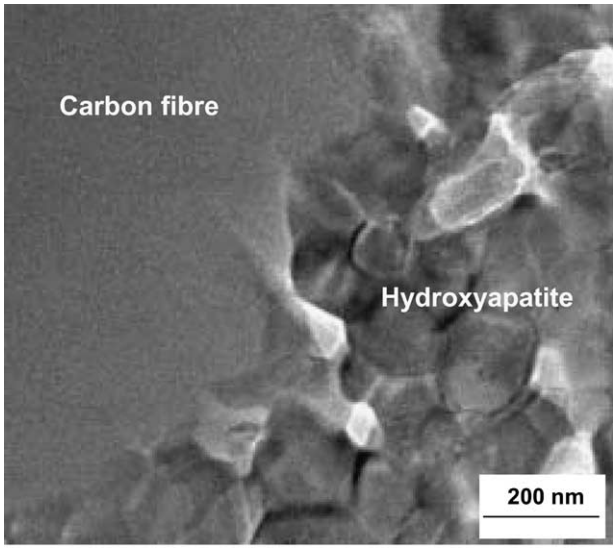


Fig. 9. Interface between carbon fibre and hydroxyapatite matrix, TEM.

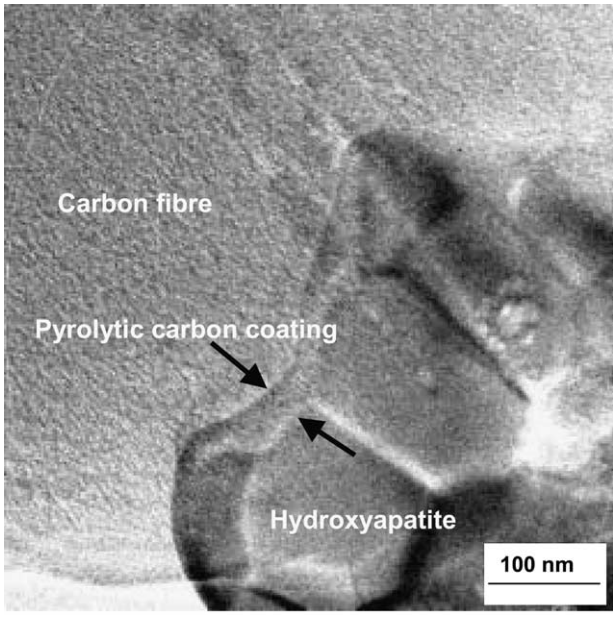


Fig. 10. Coated carbon fibre and hydroxyapatite after sintering at 1000 °C, HR-TEM.

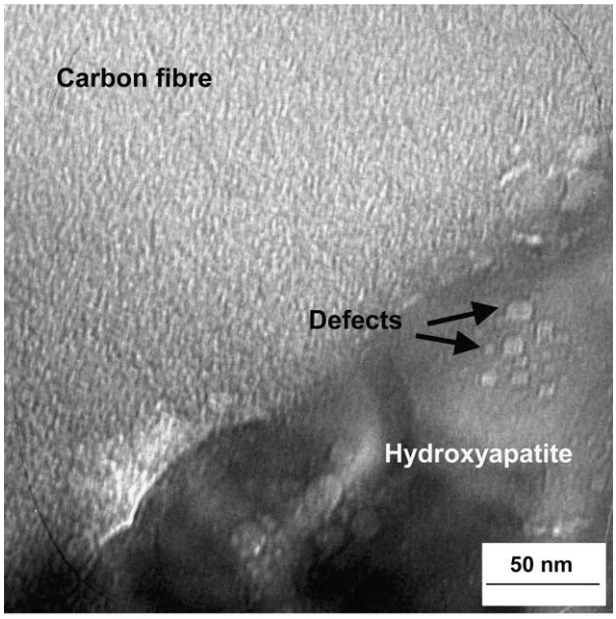


Fig. 11. Uncoated carbon fibre and hydroxyapatite after sintering at 1000 °C, HR-TEM.

hydroxyapatite. With increasing hot pressing temperature, the wear coefficient increases for the unreinforced bioceramic. It can be considered as approximately constant for the calcium phosphates with uncoated fibres. For the hydroxyapatite with pyC-coated fibres, there is a strong improvement of the wear resistant with increasing sintering temperature.

Figs. 13 and 14 show the worn surface of unreinforced hydroxyapatite sintered at 1000 °C. There are crater-like traces and scratches visible which roughen the prepolished surface. Scratches and tiny crater-like traces are also evident on the worn surface of the fibre reinforced hydroxyapatite (Fig. 15). However, the scratches are shorter in comparison to the unreinforced ceramic. In contrast to the brittle dense hydroxyapatite matrix of the composites, there are no wear traces and damage visible on the fibre surface. A few hundred nanometer thick layer of hydroxyapatite remains on the surface of the fibres (Fig. 16), but the more brittle hydroxyapatite is worn away around the fibres, even through, the fibres have a close interfacial contact to the matrix. The same observations can be made on the composites with pyC-coated fibres (Fig. 17).

Table 1
Hardness and wear coefficient of the unreinforced and short fibre reinforced hydroxyapatite

| Sample | Sintering temperature $T_s$ (°C) | Hardness (GPa) | Wear coefficient $k$ ($10^{-5}$ mm$^{-2}$ N$^{-1}$) |
|---|---|---|---|
| Hydroxyapatite | 1000 | 0.73±0.02 | 0.155±0.053 |
| | 1075 | 0.64±0.01 | 0.156±0.041 |
| | 1150 | 0.63±0.01 | 0.177±0.047 |
| Hydroxyapatite with uncoated carbon fibres | 1000 | 0.34±0.01 | 0.078±0.029 |
| | 1075 | 0.53±0.02 | 0.087±0.025 |
| | 1150 | 0.43±0.01 | 0.079±0.033 |
| Hydroxyapatite with pyC-coated carbon fibres | 1000 | 0.34±0.01 | 0.073±0.016 |
| | 1075 | 0.50±0.02 | 0.054±0.022 |
| | 1150 | 0.42±0.01 | 0.019±0.012 |

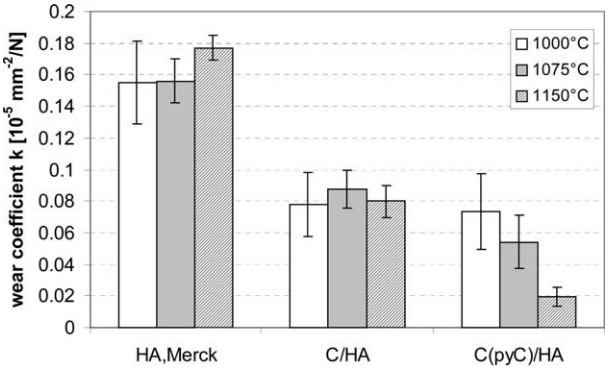


Fig. 12. Wear coefficient of calcium phosphate ceramic and composites: HA: unreinforced hydroxyapatite, C/HA: carbon fibre reinforced hydroxyapatite (carbon fibres without coating), C(pyC)/HA: carbon fibre reinforced hydroxyapatite (carbon fibres with additional pyrolytic carbon coating).

## 4. Discussion

In general, the reinforcement of hydroxyapatite with 20 vol.% carbon fibres improves the resistance of the bioceramic against microabrasion if the microstructure of the composite is adapted. Although, the graphitic carbon fibres have a lower hardness in comparison to the hydroxyapatite ceramic, they have a higher damage tolerance. In the brittle hydroxyapatite matrix, cracks move progressively and the size of critical defects, which are starting points for crack propagation, is low. The atomic and microstructural build up of graphite allows

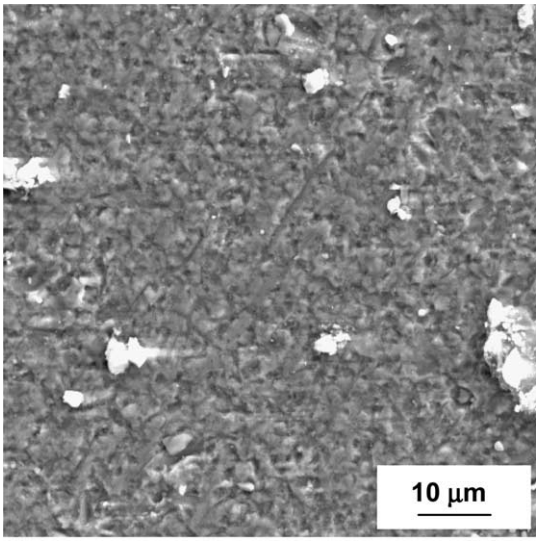


Fig. 13. Unreinforced HA, $T_s$ = 1000 °C: worn, surface, SEM.

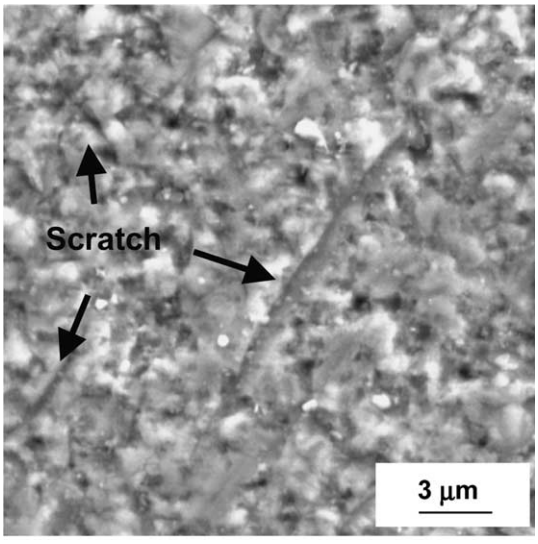


Fig. 14. Scratches and craters on unreinforced HA, SEM.

energy dissipation without a destruction of the lattice. The basal graphitic planes can be shifted against each other easily without generation of defects. As observed on the worn surface, the carbon fibres are more resistant against the indentation of the microparticles during the wear test.

The phase composition of the unreinforced and the fibre reinforced hydroxyapatite was identified as similar. No decomposition products were found and the calcium hydroxyapatite, which showed evidence of carbonate substitution, consists of fine crystalline grains without any amorphous fraction. A slight difference is observed between unreinforced and carbon fibre reinforced materials. FT-IR measurements confirmed promotion of the loss of crystal water in all composites. It is reported, that the presence of reinforcements in calcium hydroxyapatite promotes the decomposition.[11,12] Because dehydroxylation is considered as a preliminary stage of decomposition, the measured loss of crystal water is an additional hint to this phenomenon.

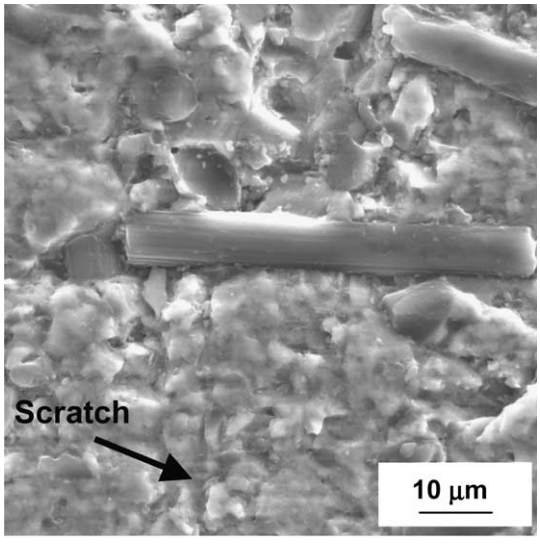


Fig. 15. Carbon fibres in HA matrix, $T_s = 1000$ °C: worn surface, SEM.

Although, microstructural features like the fibre volume fraction, the porosity or the matrix phase composition are similar for the hydroxyapatite with uncoated and with pyC-coated carbon fibres, the sensitivity against microabrasion is clearly different. A microstructural feature which is dissimilar is the crack net, which was only observed in hydroxyapatite with uncoated fibres. The symmetry structure of hydroxyapatite leads to an anisotropy in the thermal expansion coefficient.[13] The reported thermal expansion coefficient along the crystallographic axes vary from $\alpha_a = 14.1 \times 10^{-6}$ $K^{-1}$ and $\alpha_c = 21.9 \times 10^{-6}$ $K^{-1}$ [14] to $\alpha_a = 11.8 \times 10^{-6}$ $K^{-1}$ and $\alpha_c = 11.4 \times 10^{-6}$ $K^{-1}$.[14] Due to this thermal expansion anisotropy of the crystalline lattice, already sintered hydroxyapatite can have a high density of internal defects. Additionally, there is an immense difference between the thermal expansion coefficient of hydroxyapatite and the carbon fibres. The thermal expansion coefficient of carbon fibres is of between $-0.1$ and $+1.0 \times 10^{-6}$ $K^{-1}$. This drastic difference in thermal expansion leads to the observed crack net in the composites with uncoated fibres. In the case of a reinforcement with pyC-coated fibres, no crack net occurs. Obviously, the internal stresses can relax due to the interfacial pyrolytic carbon layer. The microstructure of this carbon layer differs from the oriented graphitic carbon in the fibres. In the pyC-coatings the graphitic basal planes of $sp^2$-hybridised carbon are oriented isotropic without any preferred orientation. In the case of such an isotropic orientation, a sufficient amount of

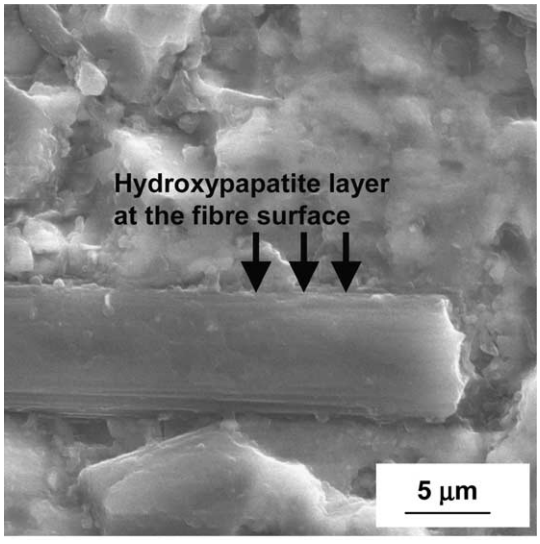


Fig. 16. Uncoated carbon fibre in HA, SEM.

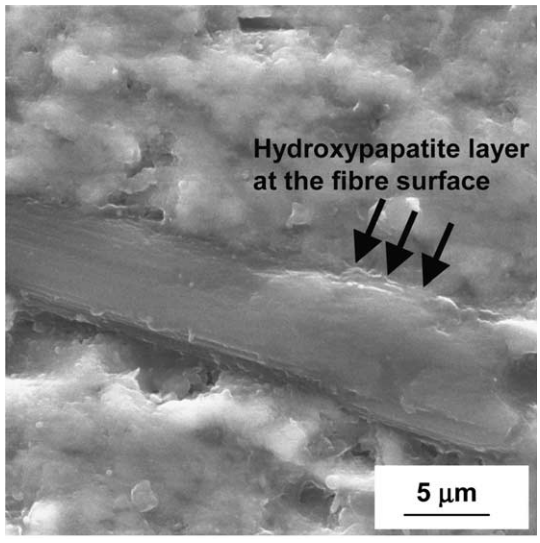


Fig. 17. Carbon fibre with pyrolytic C-coating in HA, SEM.

basal planes are positioned in a way which allows stick–slip effects, which are nano- or micro-movements between the basal planes. These stick–slip effects lead to a certain damage tolerance and buffer the stresses during the cooling of the composite.

As mentioned before, for all composites the resistance against microabrasion is improved. However, the composites with the pyC-coated fibres achieved the best results. A crack net eases the fracture of the brittle ceramics due to the impact of abrasive SiC-particles and with this the wear. The ability to reduce internal stresses by a stress consuming pyrolytic carbon coating and the subsequent absence of defects like cracks is a possible reason for the reduced sensitivity against wear.

## 5. Conclusions

Hot pressing at adjusted parameters (1000–1150 °C, 25 MPa, 15 min) allows the processing of a fine grained crystalline calcium hydroxyapatite matrix without any decomposition products. At the fibre–matrix interface, a close contact between the slightly curved fibre surface and hydroxyapatite grains was achieved, but no reaction occurred.

The reinforcement of calcium hydroxyapatite with 20 vol.% carbon short fibres positively improves the resistance against microabrasion. Additional improvements of the wear behaviour can be reached, if the microstructure is optimised. A critical factor seems to be the mismatch between thermal expansion of reinforcement and matrix. In the case of carbon fibres with preferred orientation of the graphitic basal planes, a 60 nm thick buffer layer of pyrolytic carbon with an isotropic orientation of the sixfold carbon rings is advantageous and successful in preventing crack formation. Composites with pyC-coated carbon fibres reached the best wear resistance.

## Acknowledgements

The authors are grateful to the German Research Society (Deutsche Forschungsgemeinschaft) for financial support of the projects Do 660/7-1 and Do 660/7-2. Additionally, the authors are thankful to Ms. G. Fritsche for discussion about XRD (Technische Universität Chemnitz), Professor G. Irmer for carrying out Raman spectroscopy and Dr. V. Klemm for support in HR-TEM (Technische Universität Bergakademie Freiberg).

## References

1. Buchanan, J. M., *Key Engineering Materials*, 2002, **218/220**, 487–489.
2. Fu, Y., Batchelor, A. W. and Khor, K. A., *J. Mater. Sci. Lett.*, 1998, **17**, 1695–1696.
3. Adolfsson, E. and Hermansson, L., *J. Mater. Sci.*, 2000, **35**, 5719–5723.
4. Chaki, T. K. and Wang, P. E., *J. Mater. Sci.: Mater. Med.*, 1994, **5**, 533–542.
5. Ioku, K., Somiya, S. and Yoshimura, M., *J. Ceram. Soc. Jp.*, 1991, **99-101**, 13–20.
6. De With, G. and Corbijn, A. J., *J. Mater. Sci.*, 1989, **24**, 3411–3415.
7. Knepper, M., Moricca, S. and Milthrope, B. K., *Biomaterials*, 1997, **18**, 1523–1529.
8. Slosarczyk, A., Klisch, M., Blazewicz, M., Piekarczyk, J., Stobierski, L. and Rapacz-Kmita, A.. *J. Eur. Ceram. Soc.*, 2000, 1397–1402.
9. Nestler, K., Dietrich, D., Preidel, A., Weise, K., Stöckel, S., Meyer, N. and Marx, G., *Journal de Physique IV*, 1999, **9**, 1123–1130.
10. Wang, P. E. and Chaki, T. K., *J. Mater. Sci.: Mater. Med.*, 1993, **4**, 150–158.
11. Dorner-Reisel, A., Klemm, V., Irmer, G. and Müller, E., *Biomed. Techn.*, 2002, **47**, 393–396.
12. Knepper, M., Moricca, S. and Milthrope, B. K., *Biomaterials*, 1997, **19-23**, 1523–1529.
13. Hoepfner, T. P. and Case, E. D., In *Bioceramics: Materials and Applications III, Vol. 110, Ceramic Transactions*, ed. L. George, R. P. Rusin, G. S. Fischman and V. Janas, 2000, pp. 53–66
14. Fischer, G. R., Bardhan, P. and Geiger, J. E., *J. Mater. Sci. Lett.*, 1983, **2**, 577–578.